REGULAR PAPER

Mode analysis of GaN two-dimensional photonic crystal nanocavities undercut by photo-electrochemical etching

To cite this article: T. Tajiri *et al* 2023 *Jpn. J. Appl. Phys.* **62** SG1019

Japanese Journal of Applied Physics **62**, SG1019 (2023)
https://doi.org/10.35848/1347-4065/acba80

REGULAR PAPER

Mode analysis of GaN two-dimensional photonic crystal nanocavities undercut by photo-electrochemical etching

T. Tajiri*, M. Yoshida, S. Sosumi, K. Shimoyoshi, and K. Uchida

The University of Electro-Communications, 1-5-1 Chofugaoka, Chofu, Tokyo 182-8585, Japan

*E-mail: ttajiri@uec.ac.jp

Received December 12, 2022; revised January 26, 2023; accepted February 7, 2023; published online March 3, 2023

GaN two-dimensional (2D) photonic crystal nanocavities with a single embedded InGaN quantum well are undercut by photo-electrochemical (PEC) etching and optically characterized to investigate the fundamental mode. The PEC etching selectively removes an InGaN-based sacrificial layer to form air-suspended GaN photonic crystal cavity slabs. We investigated the resonant modes of the photonic crystal nanocavities by micro-photoluminescence spectroscopy measurement at room temperature. The wavelengths of the measured resonant peaks and their dependence on the photonic crystal period agreed well with numerical analysis, allowing us to determine the fundamental mode in the measured spectra. The highest quality factor for the fundamental mode reached 3400 at blue wavelengths. This work would contribute to the improvement of GaN 2D photonic crystal nanocavities using PEC etching as well as their applications towards integrated light sources in visible wavelengths.

1. Introduction

III-nitride (N) semiconductors, with direct bandgaps of controllable widths through molar ratio of group III elements, are promising for optoelectronic device applications in visible and UV wavelengths. Light emitting and laser diodes using III-N semiconductors have been highly developed and become major light sources especially in green, blue and UV wavelengths.[1–3] In addition, large exciton binding energies in III-N semiconductors enable room temperature operation of quantum light sources.[4] For further improvement of these light sources, combination with various nanophotonic structures have been studied.[5] Improvement of extraction efficiencies of light sources were studied by introducing planar photonic structures.[6–9] Also, photonic crystals embedded together with InGaN active layers inside vertical cavities realized high power laser diodes.[10] Moreover, recent advancements in optical meta-surfaces[11,12] realized various optical components which would also improve the light sources in terms of performance and functionality.

Among various nanophotonic applications using III-N semiconductors, integrated photonics[13–19] is one of the active fields of research. Micro-scale lasers[20–25] and integration of laser sources[26–30] are extensively studied in visible and UV wavelengths using III-N semiconductors. Of particular importance for the light sources is micro-cavities[31] with small mode volumes and high quality factors (Q-factors).[32] Strong light confinement with micro-cavities can enhance light emission,[33] leading to improvement of device performance such as lower thresholds of laser sources. Among various types of micro-cavities, photonic crystal cavities fabricated in air-suspended thin slabs are especially interesting. Light confinement within the volume of the order of cubic wavelength can be realized by such photonic crystal cavities.[31] Moreover, control of modal distribution by fine-tuning cavity designs can offer enhancement of Q-factors while maintaining the small modal volume.[34]

Towards improvement of the Q-factors, fabrication methods have been studied for III-N semiconductor photonic crystal cavities.[35–50] One of the main difficulties arises from the high inertness of III-N semiconductors, which hinders undercut etching to form air-suspended photonic crystal cavity slabs by simple chemical etching. Among various undercut methods studied so far, bandgap selective photo-electrochemical (PEC) etching of InGaN-based sacrificial layers is a well-known method for the fabrication of GaN photonic crystal cavities.[22,23,35–37] Current crystal growth technology allows direct growth of GaN slab layers on InGaN-based sacrificial layers without buffer layers, which is important for the fabrication of GaN photonic crystal slabs of high crystal quality without limitation on slab thickness. Lasing oscillations were reported for GaN 1D and 2D photonic crystal cavities fabricated using this technique.[22,23] However, in comparison to other undercut methods, Q-factors of GaN 2D photonic crystal cavities fabricated by this method still remain low.[32] One reason for the low Q-factors can be due to the inadequacy of mode analysis for GaN 2D photonic crystal nanocavities fabricated by PEC etching. In particular, investigation of the fundamental mode, which typically exhibits higher Q-factors than other higher-order modes, has not been reported. Therefore, identification of the fundamental mode and evaluation of the Q-factor would be important for GaN 2D photonic crystal cavities undercut by PEC etching. We reported that a relatively high Q-factor of 1100 was obtained at blue wavelengths for GaN 2D photonic crystal nanocavities undercut by PEC etching and suggested that the resonant mode was attributed to the fundamental mode.[51]

In this paper, we report a systematic analysis on the resonant modes of GaN 2D photonic crystal nanocavities undercut by PEC etching to pinpoint the fundamental mode. The photonic crystal structures were fabricated by electron-beam (EB) lithography followed by reactive ion etching, then undercut by PEC etching to suspend the structure in the air. The PEC etching was performed by irradiation of UV laser light to samples in an acid solution. We investigated the resonant modes of the nanocavities by micro-photoluminescence (μ-PL) spectroscopy for an embedded single InGaN QW. Wavelength shifts of resonant modes in accordance with the photonic crystal period reasonably agreed with our 3D finite-difference time-domain (FDTD) calculation. The Q-factors estimated for the fundamental mode reaches 3400 at blue wavelengths. Optimization of the cavity design and the fabrication process could further improve the Q-factor, which would lead to integrated light source applications in visible wavelengths using PEC etching.

2. Experimental methods

2.1. GaN photonic crystal nanocavity structure and fabrication process

The GaN photonic crystal nanocavity structure studied is shown in Fig. 1(a). Air holes arranged in a triangular lattice are formed in the plane of a GaN slab with 120 nm thickness. The radius of the holes r and the period of the photonic crystal lattice a are given in Fig. 1(a). A cavity structure so-called L7 cavity is made by the removal of seven air holes arranged consecutively in line along the x-direction [see Fig. 1(a)]. This design is adapted because the highest Q among GaN 2D photonic crystal cavities fabricated by PEC etching was reported for an L7 cavity.[35] For fabrication of the photonic crystal cavity, we prepared a substrate in Fig. 1(b). A 220 nm thick InGaN/GaN superlattice (SL) and a 120 nm thick GaN slab containing an InGaN QW are sequentially grown on a c-plane sapphire substrate by metal–organic chemical vapor deposition. We insert another SL of high InN molar ratio at the backside of the slab as shown in Fig. 1(b) to suppress excited careers drift to the slab during the PEC undercut process. The holes of the photonic crystal are formed by reactive ion etching using Cl_2 and BCl_3 gases through a SiO_2 hard mask defined by EB-lithography. Then, the samples undergo a PEC etching for selective removal of the SL layers. During the PEC etching, the sample is immersed in an HCl-based acid solution together with a Pt electrode under an applied voltage. Pulsed laser at 375 nm wavelengths is irradiated with an optical power of 50 μW to the sample for 40 min at the repetition rate of 2 MHz. Finally, we remove the SiO_2 hard mask by HF solution.

2.2. μ-PL spectroscopy setup for optical characterization

For optical characterization of the undercut photonic crystal cavities, μ-PL spectroscopy measurement is performed at room temperature using CW He-Cd laser as the excitation source. The laser is focused on the cavities with an objective lens of 20-times magnification and 0.45 numerical aperture. The signal is collected by the same objective and measured by a spectrometer equipped with a Peltier-cooled CCD array. We measured the PL spectra using two diffraction gratings with different groove densities of 1200 mm^{-1} for low resolution and 2400 mm^{-1} for high resolution.

2.3. Numerical simulation setup

For numerical analysis of the GaN 2D photonic crystal nanocavity structure in Fig. 1(a), we used a 3D-FDTD method.[52] The spatial mesh size is 0.01 μm × 0.01 μm × 0.01 μm. Symmetrical boundary conditions are set for the x–z and y–z planes both of which are across the center of the photonic crystal cavity. Absorption boundary conditions using perfectly matched layers are imposed on other boundaries. The refractive index of the GaN and the air is set as 2.4 and 1.0, respectively. The influence of refractive index dispersion is not taken into account in this simulation. Also, the influence of the 1 μm thick GaN layer underneath is not included in the simulation unless otherwise mentioned.

3. Results and discussion

3.1. SEM observation of a GaN photonic crystal nanocavity undercut by PEC etching

SEM images of an undercut photonic crystal cavity slab for $a \sim 155$ nm and $r/a \sim 0.27$ are shown in Fig. 2. From the top and side views in Figs. 2(a), 2(b), we confirm that a layer underneath the photonic crystal slab is selectively removed, which forms an air-suspended structure. The total etching length by the PEC process is estimated to be 280 nm from the width of the bright region in Fig. 2(a). Figures 2(c) and 2(d) are the magnified top and side view images of the same sample. No significant roughness is observed on the surface of the photonic crystal slab from both SEM images. In Fig. 2(c), we also find structural fluctuations in the shape of the air holes. This can be caused by the proximity effect in EB-lithography and would be improved by optimizing the EB drawing pattern and the subsequent development process. From Fig. 2(d), we also confirm that the photonic crystal slab is slightly bent, and the cavity is approximately 20 nm closer to the GaN layer underneath.

3.2. Mode analysis on the GaN 2D photonic crystal nanocavities

Red and black curves in Fig. 3(a) show μ-PL spectra measured by the lower-resolution optical setup for a photonic crystal nanocavity and the substrate, respectively. The structural parameters for the photonic crystal nanocavity are estimated to be $a \sim 155$ nm and $r/a \sim 0.27$ by SEM observation. The excitation power is fixed at 20 μW. From the substrate, a light emission spectrum of the QW is observed as a broad single peak. On the other hand, several peaks with narrower linewidths are observed from the cavity in addition to the QW emission spectrum, which suggests that the peaks are attributed to resonant modes of the nanocavity. For more detailed analysis, we calculated resonant wavelengths of the nanocavity using 3D-FDTD method. The calculated results with respect to the resonant modes from the 1st to the 5th order modes are shown in Fig. 3(a) in

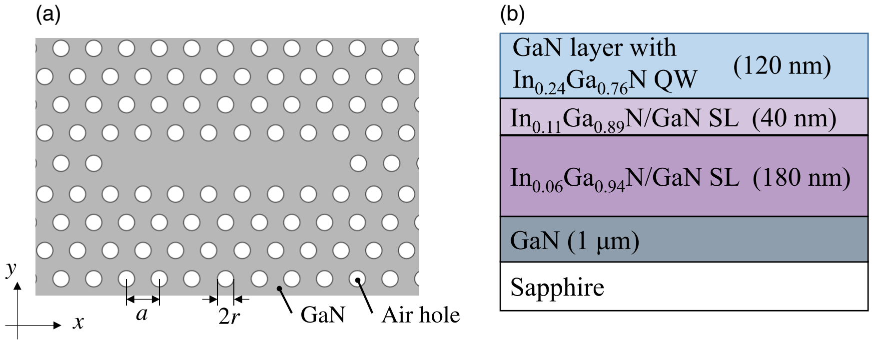

Fig. 1. (Color online) (a) Schematic top view of the studied photonic crystal nanocavity structure. Photonic crystal period a and radius of air holes r are defined in (a). (b) Schematic of the substrate structure used for fabrication of the photonic crystal nanocavities with 120 nm slab thickness.

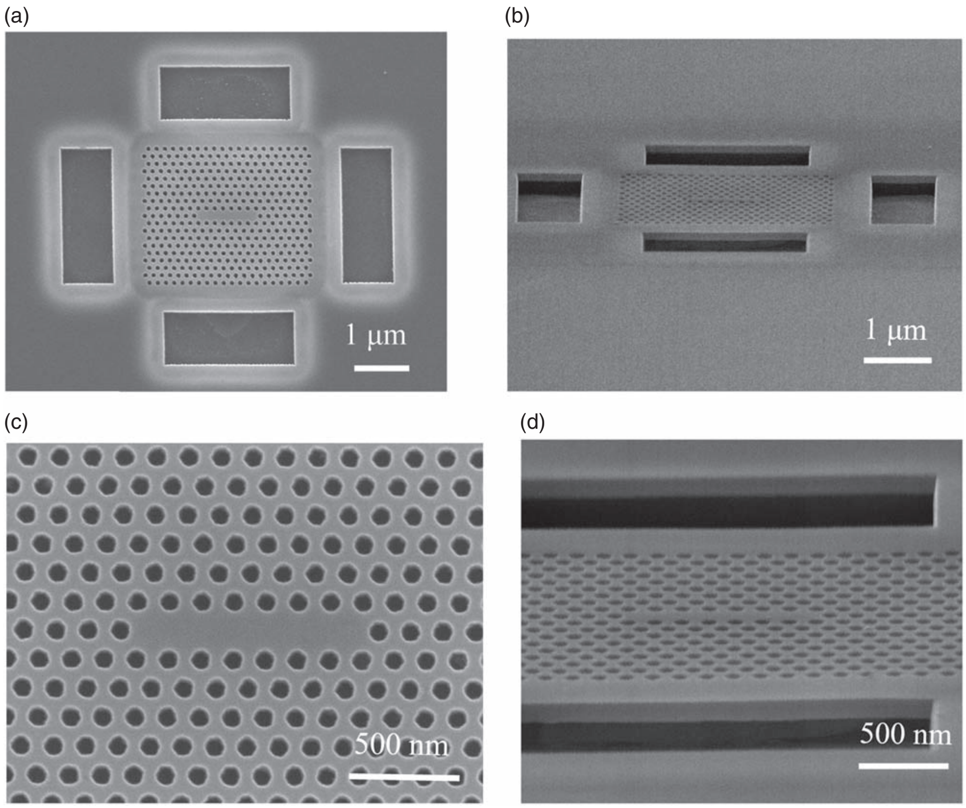

Fig. 2. SEM images of a fabricated GaN 2D photonic crystal nanocavity. Top and bird's eye views are shown in (a) and (b), respectively. The cavity region is zoomed up from the top in (c) and from an oblique angle in (d).

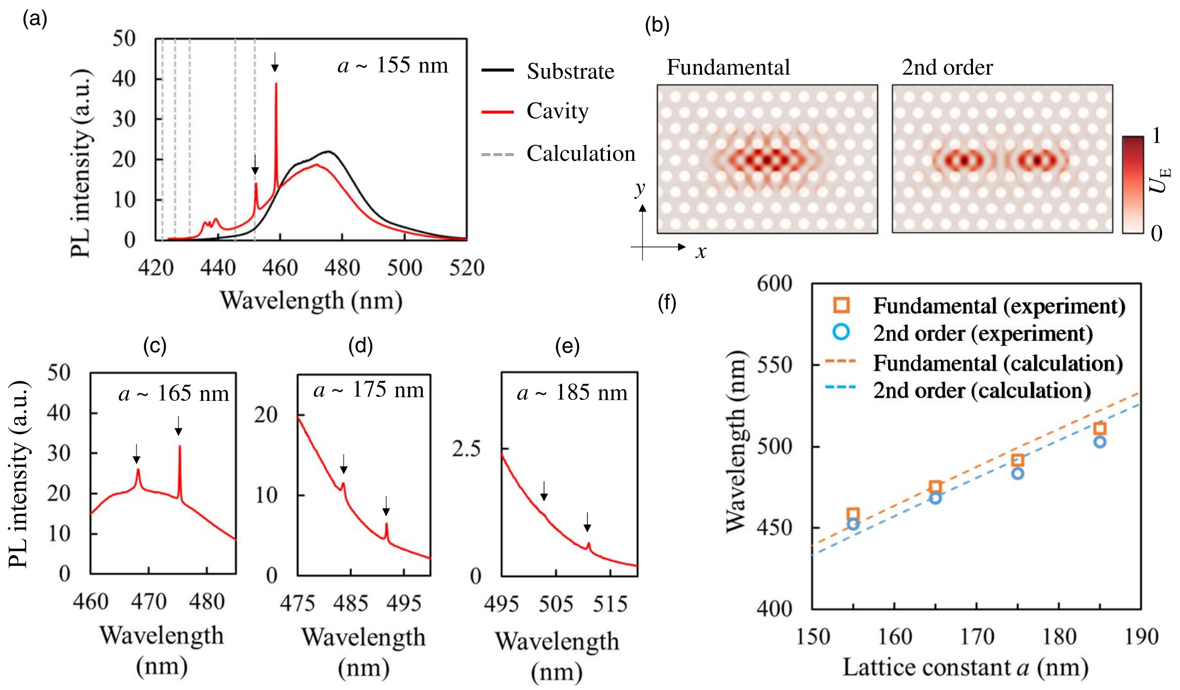

Fig. 3. (Color online) (a) μ-PL spectrum for a photonic crystal cavity of $a \sim 155$ nm (red) and for the unprocessed substrate (black). Vertical dashed lines are resonant wavelengths calculated by 3D-FDTD method. (b) Calculated spatial distribution of U_E for the fundamental and the 2nd order modes. A μ-PL spectrum measured for the fundamental and the 2nd order modes is shown for (c) $a \sim 165$ nm, (d) $a \sim 175$ nm and (e) $a \sim 185$ nm. (f) Measured and calculated a dependence of resonant wavelengths for the fundamental and the 2nd order modes.

dashed lines. Although the peak wavelengths in the experiment are slightly red-shifted in comparison to the calculated results, the number of peaks and the peak intervals reasonably agree with the calculation, which allows the identification of the fundamental mode in the experiment.

We further investigated the resonant wavelengths of the 1st and the 2nd order modes [shown by arrows in Fig. 3(a)] for different as. Calculated spatial distributions of electric field energy density (U_E) for these modes are shown in Fig. 2(b). Figures 3(c)–3(e) show the PL spectra with respect to the two modes for $a \sim 165$ nm, $a \sim 175$ nm and $a \sim 185$ nm, respectively. As a is increased from 155 to 185 nm, both resonant peaks are red-shifted. Note that the peak intensity is weaker for larger as because of weak QW light emission intensity at long wavelengths. In Fig. 3(f), the resonant wavelengths for the fundamental and 2nd order modes are shown as a function of a in comparison to the results of 3D-FDTD simulation. The measured a dependence of the resonant wavelengths reasonably matched the calculation. Discrepancy between the experiment and the calculation is likely due to the refractive index dispersion of GaN. Resonant wavelengths shifts due to the dispersion of III-nitride semiconductors were also reported for 2D photonic crystal nanocavities in previous studies.[38,41]

3.3. Discussion on the *Q*-factors of the GaN 2D photonic crystal nanocavities

We investigate the Q-factors of the fundamental and 2nd order modes by Lorentzian fitting to cavity mode spectra which are measured by our higher-resolution optical setup. Figure 4(a) shows the estimated Q-factors (Q_{exp}) as a function of a. The Q_{exp} of the fundamental mode is higher than the 2nd order mode for all values of a. This relationship agrees with our 3D-FDTD simulation where the calculated Q (Q_{cal}) is almost constant at $Q_{cal} \sim 25\,000$ for the fundamental mode and $Q_{cal} \sim 2500$ for the 2nd order mode regardless of a. The maximum Q_{exp} reaches 3400 for $a \sim 165$ nm as shown by the fitted Lorentz function for the cavity mode spectrum in Fig. 4(b). To the best of our knowledge, this would be the first report on Q-factors of the fundamental mode for GaN 2D photonic crystal nanocavities undercut by PEC etching.

On the other hand, there is a large discrepancy between the calculation and the experiment for the dependence of Q of the fundamental mode on a. The Q_{exp} is suddenly reduced for a smaller than 165 nm while the reduction is moderate for larger as. Although a more detailed investigation will be required for understanding this behavior, we consider the discrepancy caused in part by the influence of the 1 μm thick GaN layer underneath. In 3D-FDTD simulation including the underlying GaN layer, the calculated Q for the fundamental mode is $Q_{cal} \sim 14\,000$ for $a = 155$ nm, and linearly decreases to $Q_{cal} \sim 5800$ for $a = 185$ nm due to evanescent coupling to the underlying GaN layer. This a dependence of Q_{cal} is similar to that of Q_{exp} for $a \sim 165$ nm to $a \sim 185$ nm, where Q_{exp} decreases with increasing a as shown in Fig. 4(a). This suggests that the evanescent coupling loss could be dominant in this range for the fundamental mode. Difference between the Q_{cal} and the Q_{exp} for this a range may be caused by fabrication imperfections such as fluctuations in the shape of air holes in our photonic crystal nanocavities [see Fig. 2(c)] and slight bending of photonic crystal slabs.

The evanescent coupling loss could also influence the 2nd order mode. When the GaN layer underneath is taken into account, Q_{cal} for the 2nd order mode decreases from $Q_{cal} \sim 2400$ to $Q_{cal} \sim 1600$ as a increases from 155 nm to 185 nm. Thus, this reduction of Q_{cal} as well as fabrication imperfections could be the main reason for reduction of Q_{exp} at $a \sim 185$ nm for the 2nd order mode in Fig. 4(a).

Aside from evanescent coupling, another optical loss mechanism is predicted for the low Q_{exp} of the fundamental mode at $a \sim 155$ nm where the evanescent coupling calculated from the 3D-FDTD simulation is expected to be weak. One possible reason would be optical absorptions by the InGaN QW. For small a, the resonant wavelength of the fundamental mode is shorter than the QW emission peak [see Fig. 3(a)]. Under this condition, QW absorption can be as strong as reported in previous studies on GaN micro-disk cavities.[53,54] This suggests that optical absorptions by the InGaN QW could be the dominant loss at $a \sim 155$ nm for the fundamental mode and result in the low Q_{exp} in Fig. 4(a). Improvement of the cavity design as well as optimization of the fabrication process would further improve the Qs of GaN photonic crystal nanocavities undercut by PEC etching.

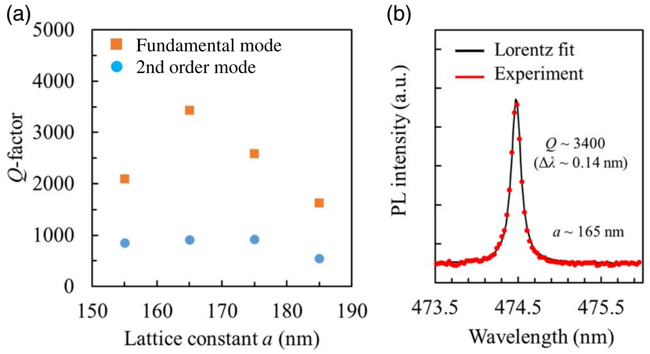

Fig. 4. (Color online) (a) Measured Q-factors for photonic crystal nanocavities with different as from 155 to 185 nm. The Qs for the fundamental and the 2nd order modes are shown with orange squares and blue circles, respectively. (b) Cavity mode spectrum (red circles) and fitted Lorentz function (black line) for the fundamental mode of a photonic crystal nanocavity with $a \sim 165$ nm.

4. Conclusions

In conclusion, we have investigated GaN 2D photonic crystal nanocavities undercut by PEC etching and analyzed the resonant modes. We fabricate the photonic crystal structures by electron-beam lithography and reactive ion etching, then undercut them by PEC etching using a UV laser source. SEM observation of the fabricated structure shows that undercut etching was accomplished by our PEC process. Resonant modes of the fabricated nanocavities are observed by micro-photoluminescence spectroscopy measurement. The wavelength shifts for the fundamental and the 2nd order modes shows a reasonable agreement with 3D-FDTD calculations. Measured Q-factors for the fundamental mode reaches $Q \sim 3400$ which is the highest among GaN 2D photonic crystal nanocavities undercut by PEC etching. We believe that this work will be an important step towards the improvement of GaN 2D photonic crystal nanocavities by PEC etching, and paves the way towards integrated light source applications in visible wavelengths.

Acknowledgments

This work was supported by JSPS KAKENHI Grant Number 20K1478, the Amada foundation, Yazaki Memorial Foundation for Science and Technology, and the Mazda Foundation. The authors fabricated samples at the Division of Advanced Research Facilities (DARF) and Key Research Facilities (KRF) of the Coordinated Center for UEC Research Facilities.

1) D. Feezell and S. Nakamura, C. R. Physique **19**, 113 (2018).
2) H. S. Wasisto, J. D. Prades, J. Gulink, and A. Waag, Appl. Phys. Rev. **6**, 041315 (2019).

3) M. Kneissl, T.-Y. Seong, J. Han, and H. Amano, Nat. Photon. **13**, 233 (2019).
4) Y. Arakawa and M. Holmes, Appl. Phys. Rev. **7**, 021309 (2020).
5) M. S. Alias et al., J. Nanophoton. **12**, 043508 (2018).
6) J. J. Wierer, A. David, and M. M. Megens, Nat. Photon. **3**, 163 (2009).
7) A. David, T. Fujii, B. Moran, S. Nakamura, S. P. DenBaars, C. Weisbuch, and H. Benisty, Appl. Phys. Lett. **88**, 133514 (2006).
8) Y. Kashima et al., Appl. Phys. Express **11**, 012101 (2018).
9) S. Xia, T. Aoki, K. Gao, M. Arita, Y. Arakawa, and M. J. Holmes, ACS Photonics **8**, 1656 (2021).
10) H. Matsubara, S. Yoshimoto, H. Saito, Y. Jianglin, Y. Tanaka, and S. Noda, Science **319**, 445 (2008).
11) H. Liang, A. Martins, B.-H. V. Borges, J. Zhou, E. R. Martins, J. Li, and T. F. Krauss, Optica **6**, 1461 (2019).
12) S. M. Kamalia, E. Arbabia, A. Arbabi, and A. Faraon, Nanophotonics **7**, 1041 (2018).
13) C. Xiong, W. H. P. Pernice, X. Sun, C. Schuck, K. Y. Fong, and H. X. Tang, New J. Phys. **14**, 095014 (2012).
14) N. Li, C. P. Ho, S. Zhu, Y. H. Fu, Y. Zhu, and L. Y. T. Lee, Nanophotonics **10**, 2347 (2021).
15) T.-J. Lu et al., Opt. Express **26**, 11147 (2018).
16) T. Sekiya, T. Sasaki, and K. Hane, J. Vac. Sci. Technol. B. **33**, 031207 (2015).
17) H. Chen, H. Fu, X. Huang, X. Zhang, T.-H. Yang, J. A. Montes, I. Baranowski, and Y. Zhao, Opt. Express **25**, 31758 (2017).
18) M. Gromovyi, M. El Kurdi, X. Checoury, E. Herth, F. Tabataba-Vakili, N. Bhat, A. Courville, F. Semond, and P. Boucaud, Opt. Express **30**, 20737 (2022).
19) D. Jevtics et al., Opt. Mater. Express **11**, 3567 (2021).
20) Y. Zhang, X. Zhang, K. H. Li, Y. F. Cheung, C. Feng, and H. W. Choi, Phys. Status Solidi a **212**, 960 (2015).
21) G. Zhu, F. Qin, X. Li, Y. Sun, F. Gao, M. Tian, B. Ji, and Y. Wang, Front. Mater. **9**, 845885 (2022).
22) C.-H. Lin, J.-Y. Wang, C.-Y. Chen, K.-C. Shen, D.-M. Yeh, Y.-W. Kiang, and C. C. Yang, Nanotechnology **22**, 025201 (2011).
23) N. Niu, A. Woolf, D. Wang, T. Zhu, Q. Quan, R. A. Oliver, and E. L. Hu, Appl. Phys. Lett. **106**, 231104 (2015).
24) N. Vico Triviño, R. Butté, J.-F. Carlin, and N. Grandjean, Nano Lett. **15**, 1259 (2015).
25) S. T. Jagsch et al., Nat. Commun. **9**, 564 (2018).
26) K. H. Li, W. Y. Fu, and H. W. Choi, Prog. Quantum Electron. **70**, 100247 (2020).
27) R. Arefin, S. H. Ramachandra, H. Jung, W. You, S. M. N. Hasan, H. Turski, S. Dwivedi, and S. Arafin, IEEE J. Quantum Electron. **56**, 6300309 (2020).
28) T. Kamei, T. Kamikawa, M. Araki, S. P. DenBaars, S. Nakamura, and J. E. Bowers, Phys. Status Solidi a **217**, 1900770 (2020).
29) F. Tabataba-Vakili et al., ACS Photonics **5**, 3643 (2018).
30) F. Tabataba-Vakili et al., Opt. Lett. **45**, 4276 (2020).
31) K. J. Vahala, Nature **424**, 839 (2003).
32) R. Butté and N. Grandjean, Nanophotonics **9**, 569 (2020).
33) E. M. Purcell, Phys. Rev. **69**, 681 (1946).
34) Y. Akahane, T. Asano, B.-S. Song, and S. Noda, Nature **425**, 944 (2003).
35) Y.-S. Choi, K. Hennessy, R. Sharma, E. Haberer, Y. Gao, S. P. DenBaars, S. Nakamura, E. L. Hu, and C. Meier, Appl. Phys. Lett. **87**, 243101 (2005).
36) C. Meier, K. Hennessy, E. D. Haberer, R. Sharma, Y.-S. Choi, K. McGroddy, S. Keller, S. P. DenBaars, S. Nakamura, and E. L. Hu, Appl. Phys. Lett. **88**, 031111 (2006).
37) P. D. Anderson, A. J. Fischer, D. D. Koleske, B. P. Gunning, and G. Subramania, Opt. Mater. Express **8**, 3543 (2018).
38) M. Arita, S. Ishida, S. Kako, S. Iwamoto, and Y. Arakawa, Appl. Phys. Lett. **91**, 051106 (2007).
39) S. Blumenthal, M. Bürger, A. Hildebrandt, J. Förstner, N. Weber, C. Meier, D. Reuter, and D. J. As, Phys. Status Solidi c **13**, 292 (2016).
40) D. Néel et al., Appl. Phys. Lett. **98**, 261106 (2011).
41) N. Vico Triviño, G. Rossbach, U. Dharanipathy, J. Levrat, A. Castiglia, J.-F. Carlin, K. A. Atlasov, R. Butté, R. Houdré, and N. Grandjean, Appl. Phys. Lett. **100**, 071103 (2012).
42) D. Sam-Giao et al., Appl. Phys. Lett. **100**, 191104 (2012).
43) F. Tabataba-Vakili et al., Appl. Phys. Lett. **111**, 131103 (2017).
44) M. Arita, S. Kako, S. Iwamoto, and Y. Arakawa, Appl. Phys. Express **5**, 126502 (2012).
45) T.-T. Wu, S.-Y. Lo, H.-M. Huang, C.-W. Tsao, T.-C. Lu, and S.-C. Wang, Appl. Phys. Lett. **102**, 191116 (2013).
46) S. Ichikawa, Y. Sasaki, T. Iwaya, M. Murakami, M. Ashida, D. Timmerman, J. Tatebayashi, and Y. Fujiwara, Phys. Rev. Appl. **15**, 034086 (2021).
47) T. Iwaya, S. Ichikawa, D. Timmerman, J. Tatebayashi, and Y. Fujiwara, Opt. Express **30**, 28853 (2022).
48) S. Sergent, M. Arita, S. Kako, K. Tanabe, S. Iwamoto, and Y. Arakawa, Appl. Phys. Lett. **101**, 101106 (2012).
49) S. Sergent, M. Arita, S. Kako, K. Tanabe, S. Iwamoto, and Y. Arakawa, Phys. Status Solidi c **10**, 1517 (2013).
50) I. Rousseau, I. Sánchez-Arribas, K. Shojiki, J.-F. Carlin, R. Butté, and N. Grandjean, Phys. Rev. B **95**, 125313 (2017).
51) M. Yoshida, S. Sosumi, K. Shimoyoshi, K. Uchida, and T. Tajiri, Int. Microprocesses and Nanotechnology Conf. Digest Papers 2022, 10D–1–4.
52) A. Oskooi, D. Roundy, M. Ibanescu, P. Bermel, J. D. Joannopoulos, and S. G. Johnson, Comput. Phys. Commun. **181**, 687 (2010).
53) D. Simeonova, E. Feltin, A. Altoukhov, A. Castiglia, J.-F. Carlin, R. Butté, and N. Grandjean, Appl. Phys. Lett. **92**, 171102 (2008).
54) E. D. Haberer, C. Meier, R. Sharma, A. R. Stonas, S. P. DenBaars, S. Nakamura, and E. L. Hu, Phys. Stat. Sol. (c) **2**, 2845 (2005).